

# Nickel/Porous Carbon Composite Derived from Bimetallic MOFs for Electrical Double-Layer Supercapacitor Application

XianHe Meng<sup>1</sup>, ChuBin Wan<sup>1</sup>, SuYe Yu<sup>1</sup>, XiaoPing Jiang<sup>2</sup>, Xin Ju<sup>1,\*</sup>

<sup>1</sup> Department of Physics, University of Science and technology Beijing, Beijing, P. R. China

<sup>2</sup> Shandong Key Laboratory for High Strength Lightweight Metallic Materials, Advanced Materials Institute, Shandong Academy of Sciences, Jinan 250014, P. R. China

\*E-mail: [jux@ustb.edu.cn](mailto:jux@ustb.edu.cn)

*Received:* 11 April 2018 / *Accepted:* 8 June 2018 / *Published:* 5 July 2018

---

A novel method to synthesize nickel/ porous activated carbon composite materials has been proposed initially from bimetallic Ni(II)-MOF-5s. Electrochemical results present that the nickel /activated carbon maintains nearly 83 % capacity with the current density increases from 0.2 to 50 A g<sup>-1</sup> and shows excellent cyclic stability of about 1.5 % decrease after 5000 cycles. This product also demonstrated a good rectangularity at a high scan voltage of 2 V s<sup>-1</sup> and very low charge transfer resistance of approximately 0.35 Ω, which can be a prospective electrode material for electrochemical double-layer supercapacitor applications.

---

**Keywords:** Bimetallic MOFs; Ni nanoparticles; Graphitic porous carbon; Supercapacitor

## 1. INTRODUCTION

Over the past few decades, electrochemical double-layer capacitors (EDLCs) have been successfully applied in high-power-density energy-storage devices; EDLCs can also be used for various energy conversion applications[1-3]. Carbon-based materials are important high-performance EDLCs electrode materials due to their excellent inherent features such as high electrical conductivity, physicochemical stability, high specific surface areas, acceptable cost and environmental friendliness [4-7]. The ideal EDLC electrode materials would exhibit satisfactory conductivity and interconnected channels to accelerate ion dispersion efficiently [6-8]. However, it is crucial to design novel carbon materials to improve high-rate electrochemical processes such as electronic transport and ion diffusion in porous electrodes. Recently, one possible route for enhancing the conductivity and electrochemical performances of these materials through doping with metallic Ni via various synthetic methods has been developed [9-12]. These studies suggest that the Ni/C hybrid composite materials could enhance

the electrode/electrolyte interface interaction by accelerating the diffusion of the electrons and ions to improve the electrochemical performance.

MOFs (metal-organic frameworks) have proven to be as good precursors for highly porous carbon materials and carbon composites containing metallic or metal-oxide nanoparticles under proper pyrolysis conditions [13-15]. The desired functional micro/nanostructures without agglomeration and impurities can be easily obtained by a template pyrolysis route using MOFs with an ordered arrangement of metal ions and organic nodes. The resultant materials inherit some of the excellent qualities of the MOFs as they apply to in energy storage and conversion in devices such as lithium-ion batteries, sodium-ion batteries and electrochemical supercapacitors [15-19].

Recently, a few studies reported on increasing the diversity and functionality of MOF-5 by the effective incorporation of metal ions (such as  $\text{Co}^{2+}$ ,  $\text{Ni}^{2+}$ ) into the frameworks using one-pot or postsynthetic methods [20-23]. Here, we demonstrate a novel method to prepare highly porous Ni/C nanocomposites from bimetallic Ni(II)-doped MOF-5 cubic crystals, which are not like other similar conventional materials synthesized by simple physical mixing processes. Fig. 1 illustrates the design and application of the products. Some previous studies reported that a similar nickel/carbon composite could show pseudocapacitance characteristics in an aqueous electrolyte indicating that the metallic Ni might convert to other phases such as nickel hydroxide and nickel oxide in alkaline aqueous electrolytes [24, 25]. In our study, the synthesized porous Ni/C derived bimetallic Ni(II)-doped MOF-5 performed very well in EDLCs without faradic capacitance. This material exhibits some favorable characteristics of ideal electrochemical double-layer capacitors such as low electric transport resistance, good capacitance retention at a high rate and cyclic stability.

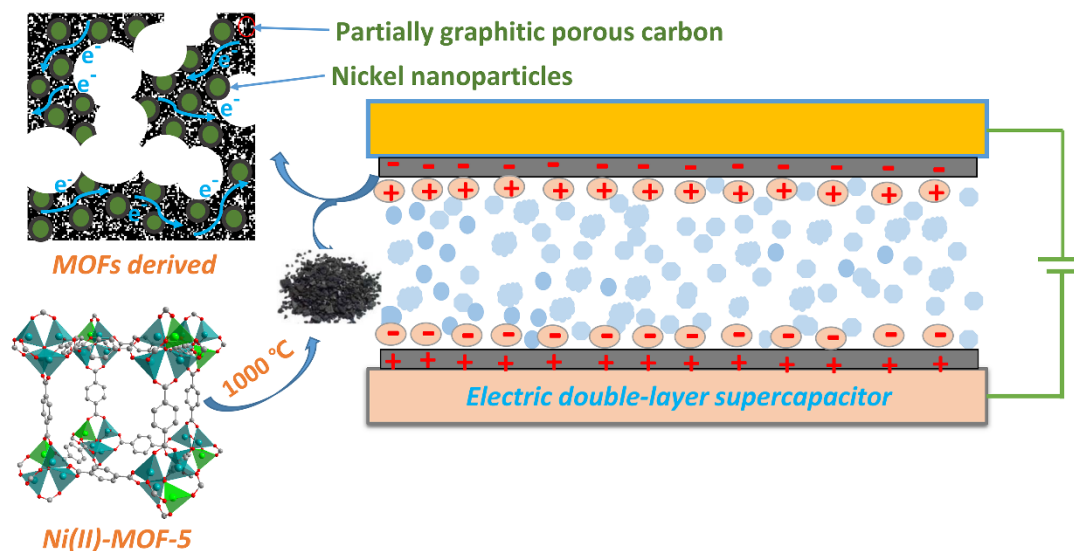


**Figure 1.** The schematic illustration of the product derived from Ni(II)-MOF-5 and application in supercapacitor.

## 2. EXPERIMENTAL

The materials preparation procedures were prepared according to our previous reported method [26]. Briefly, 0.2975 g of  $\text{Zn}(\text{NO}_3)_2 \cdot 6\text{H}_2\text{O}$  and 0.0332 g of 1,4-benzenedicarboxylic acid ( $\text{H}_2\text{BDC}$ ) were dissolved in 30 mL of N,N-dimethylformamide (DMF) and transferred into a 50mL Teflon-lined autoclave, then maintained at 120 °C for 24 h to yield white MOF-5 crystals. Light green crystals of Ni(II)-MOF-5s were synthesized using a similar procedure. To synthesize Ni1-MOF-5, we used 0.0291 g of  $\text{Ni}(\text{NO}_3)_2 \cdot 6\text{H}_2\text{O}$  together with 0.2677 g of  $\text{Zn}(\text{NO}_3)_2 \cdot 6\text{H}_2\text{O}$ , while Ni2-MOF-5 was synthesized by using 0.1454 g of  $\text{Ni}(\text{NO}_3)_2 \cdot 6\text{H}_2\text{O}$  and 0.1487 g of  $\text{Zn}(\text{NO}_3)_2 \cdot 6\text{H}_2\text{O}$ . Before obtaining the pristine MOFs powder, the as-synthesized samples were washed and immersed using DMF and  $\text{CH}_2\text{Cl}_2$  for several times, finally degassed at for 12 h at 120 °C. Solid-state calcination of MOF-5 and Ni(II)-MOF-5s powder was performed in a tube furnace at 1000 °C for 3 h under argon flow. According the previous research [27], the ZnO was formed due to the decomposition of the MOF-5 framework approximately at 500 °C, then when the temperature reached higher than 800 °C, the metallic Zn was observed from the reduction of ZnO during the carbonization process. Finally, the resulting product was composed of carbon species alone after the metallic Zn (boiling point at 908 °C) evaporating away along with the argon flow. Besides, it was noted that the nickel oxide was reduced to metallic nickel by the carbon product around at a higher temperature of 600 °C and Ni metal has higher boiling point than 1000 °C [24]. In this work, the pure activated carbon product derived from MOF-5 was denoted as AC-0, and nickel/porous carbon composite derived from bimetallic MOFs were named: Ni/AC-1, Ni/AC-2, respectively.

Cyclic voltammetry (CV) tests and chronopotentiometry were performed at room temperature on an electrochemical working station (CHI660E, Shanghai, China), using a three-electrode system in 6 M KOH aqueous electrolyte equipped with a counter electrode of Pt electrode and a reference electrode of Hg/HgO electrode. The cyclic voltammetry (CV) were obtained at a different scan rate from 0.1 to 2  $\text{V s}^{-1}$  in the potential range of -1.0~0 V. The galvanostatic charge-discharge (GC) measurements was performed from 0.2  $\text{A g}^{-1}$  to 50  $\text{A g}^{-1}$  in the potential range of -1.0~0 V. The activation materials were pressed with porous nickel foam with a coating area of 1  $\text{cm}^2$  at 10 MPa for 10s. The electrochemical impedance spectroscopy (EIS) measurements were taken in a frequency from 100 kHz to 0.01 Hz using multi-channel potentiostat/galvanostat/impedance analyzer (AMETEK VersaSTAT MC). The morphological images were obtained using field-emission scanning electron microscopy (FE-SEM, ZEISS SUPRA55 SAPPHIRE) and transmission electron microscopy (TEM, JEOL JEM-2100).

## 3. RESULTS AND DISCUSSION

Fig. 2a1, b1 and c1 shows the crystalline structure frameworks of the MOF-5, Ni1-MOF-5 and Ni2-MOF-5, respectively. The cyan structure units represent  $\text{Zn}^{2+}$  ions. The green units represent the  $\text{Ni}^{2+}$  ions that  $\text{Zn}^{2+}$  incorporate into the framework by replacing  $\text{Zn}^{2+}$  ion with different degrees of substitution.

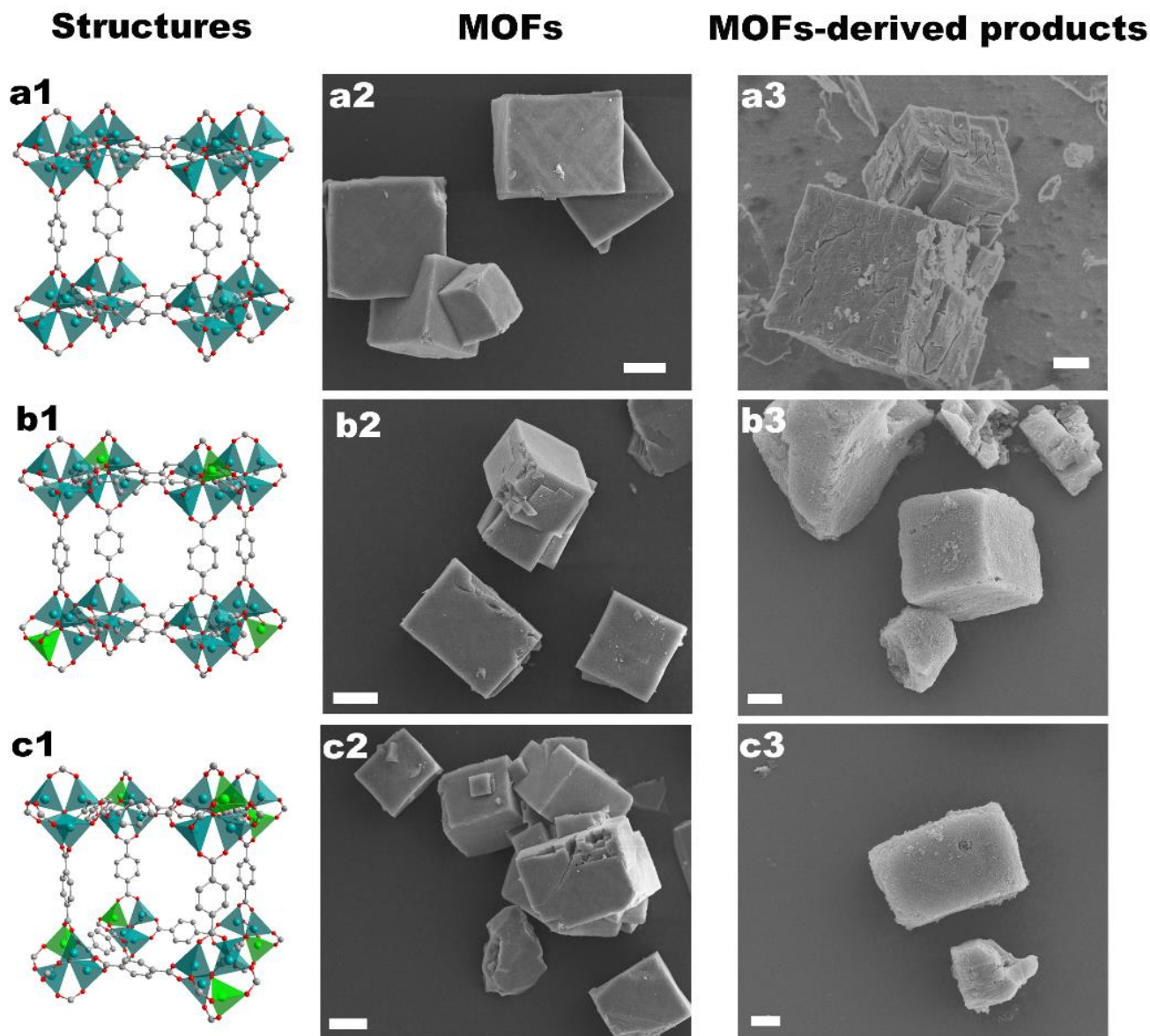


**Figure 2.** The crystal structures of (a1) MOF-5, (b1) Ni1-MOF-5, (c1) Ni2-MOF-5; SEM images of (a2) MOF-5, (b2) Ni1-MOF-5, (c2) Ni2-MOF-5, (a3) AC-0, (b3) Ni/AC-1 and (c3) Ni/AC-2 with the same scale of 10  $\mu\text{m}$ .

The number of substituted ions corresponds to the elemental ratios obtained by previous research [26]. The SEM images of MOF-5s and Ni(II)-MOF-5s are presented in Fig. 2a2, b2 and c2. The Ni(II)-MOF-5s show well-defined cubic crystal morphologies similar to the pure MOF-5, suggesting that no obvious visible feature changes occurred with the  $\text{Ni}^{2+}$  doping of MOF-5.

Fig. 3a, b and c, d show the microstructures of AC-0 and Ni/AC-2, respectively. AC-0 has an amorphous carbon microstructure and Ni/AC-2 has nickel nanoparticles embedded in the amorphous carbon. Well-dispersed Ni nanoparticles could be considered active nanocollectors set into the carbon substrate.

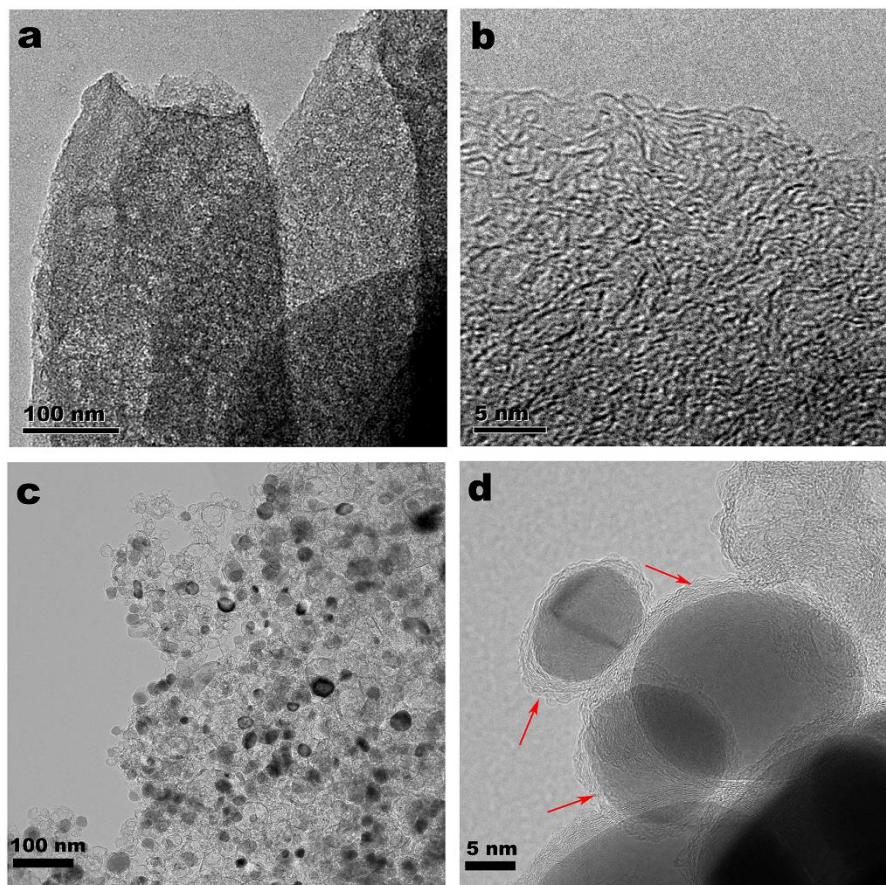


**Figure 3.** TEM images of (a, b) AC-0 and (c,d) Ni/AC-2.

Moreover, the Ni nanoparticles in nickel/carbon composite should create many interconnected channels which could play an important role in electron transport. The higher multiple TEM image in Fig. 3d indicates the appearance of some carbon shells (marked area). The generation of these turbostratic graphitic shells could be attributed to the catalytic activity of Ni in forming graphite [28]. Ni/AC-2 should have a higher degree of graphitization with more turbostratic graphitic shells when more fine and uniform Ni nanoparticles increase to some extent, which is in agreement with our previous PXRD and Raman results [26]. These characteristics suggest that the Ni/AC-2 could be a good material for EDLC electrodes.

Fig. 4 shows that the derived materials were also tested using chronopotentiometry at different current densities from 0.2 to 50 A g<sup>-1</sup>. Specific capacitance values were calculated from the galvanostatic discharge curves using the following formula:

$$C = I \Delta t / \Delta U M \quad (1)$$

where  $I$  is the discharge current,  $\Delta t$  is the discharging time and  $M$  is the mass of the activated material.  $\Delta U$  is the voltage range during the galvanostatic discharging.  $\Delta U$  can be obtained by the following formula:

$$\Delta U = U - IR \quad (2)$$

where  $IR$  is the potential drop when the current switches at the galvanostatic charge/discharge point.  $U$  is the voltage window range (V). The specific capacitances of all the sample electrodes were obtained

using Formula (1) and (2) and are summarized in Table 1. As the current densities increase from 0.2 to 50 A g<sup>-1</sup>, the specific capacitance of all the sample electrodes decreased accordingly. The AC-0, Ni/AC-1 and Ni/AC-2 electrodes exhibited specific capacitances of 165, 120, 81 F g<sup>-1</sup>, respectively, at a low current density of 0.2 A g<sup>-1</sup> and specific capacitances of 121, 92, 67 F g<sup>-1</sup>, respectively, at a high current density of 50 A g<sup>-1</sup>. From the galvanostatic charge/discharge results, the specific capacitance decreased as the current density increased due to the low rate of ion diffusion within micropores [29]. Additionally, Ni/AC exhibited a relatively lower specific capacitance than AC-0 due to the metallic Ni content increase.

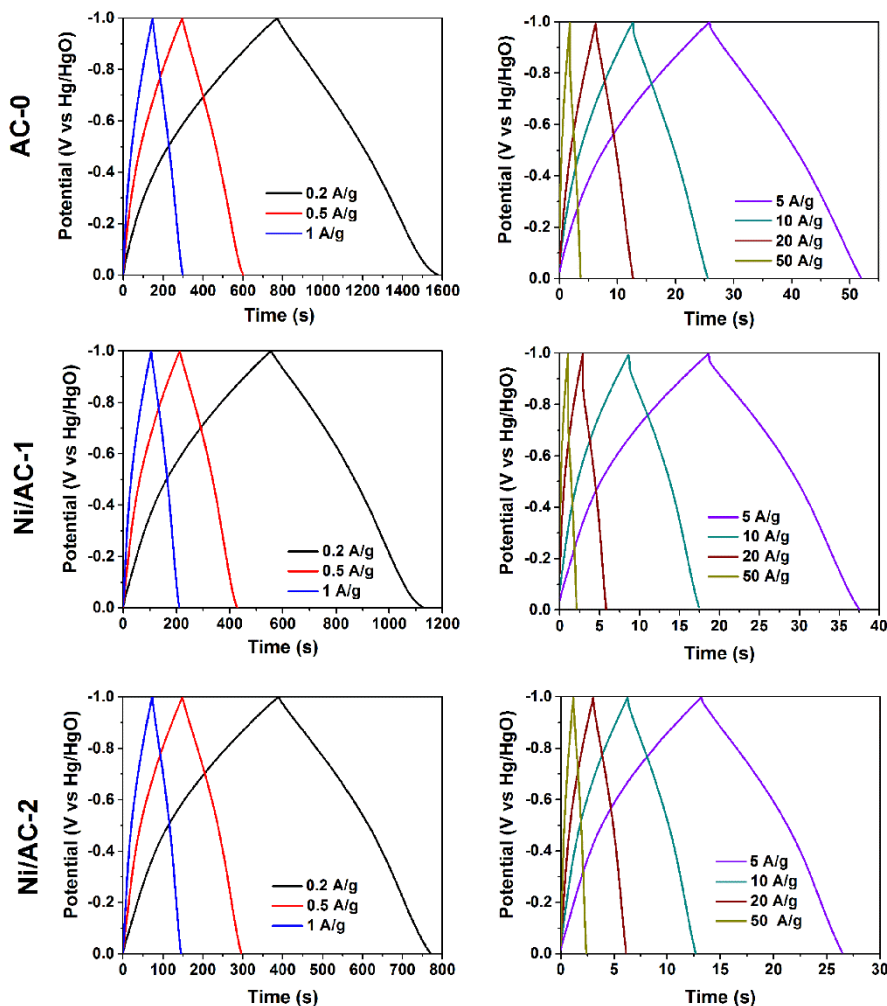


**Figure 4.** Galvanostatic charge/discharge curves of the MOFs-derived products at different current densities.

**Table 1.** Summary of the specific capacitances value obtained from Figure 4 at different current densities from 0.2 to 50 A g<sup>-1</sup>.

Sample	0.2	0.5	1	5	10	20	50	A g <sup>-1</sup>
AC-0	165	155	152	142	137	133	121	F g <sup>-1</sup>
Ni/AC-1	120	112	111	105	99	96	92	F g <sup>-1</sup>
Ni/AC-2	81	78	77	75	74	71	67	F g <sup>-1</sup>

To assess the supercapacitance performance of the materials, the cyclic voltammetry (CV) was also tested as shown in Fig. 5. For comparison, the CV of AC-0, Ni/AC-1 and Ni/AC-2 were conducted at 1 and 2  $\text{V s}^{-1}$  as shown in Fig. 5a and b. The Ni/AC-2 sample shows the most rectangular shape, which is the characteristic of ideal EDLC electrode materials. Furthermore, the CV curves of Ni/AC-2 (Fig. 5c) retain their rectangular shapes through a wide range of voltage sweep rates (0.1 to 2  $\text{V s}^{-1}$ ). The rectangular shape of the cyclic voltammetry (CV) curves is due to the rapid reorganization in the electrical double-layer at the switching potentials [30]. These electrochemical results should be attributed to the structural advantages of Ni/AC-2: fine and uniform nickel nanoparticles well-dispersed in partially graphitic porous carbon, accelerating the delivery of electrons, and thus increasing conductivity.

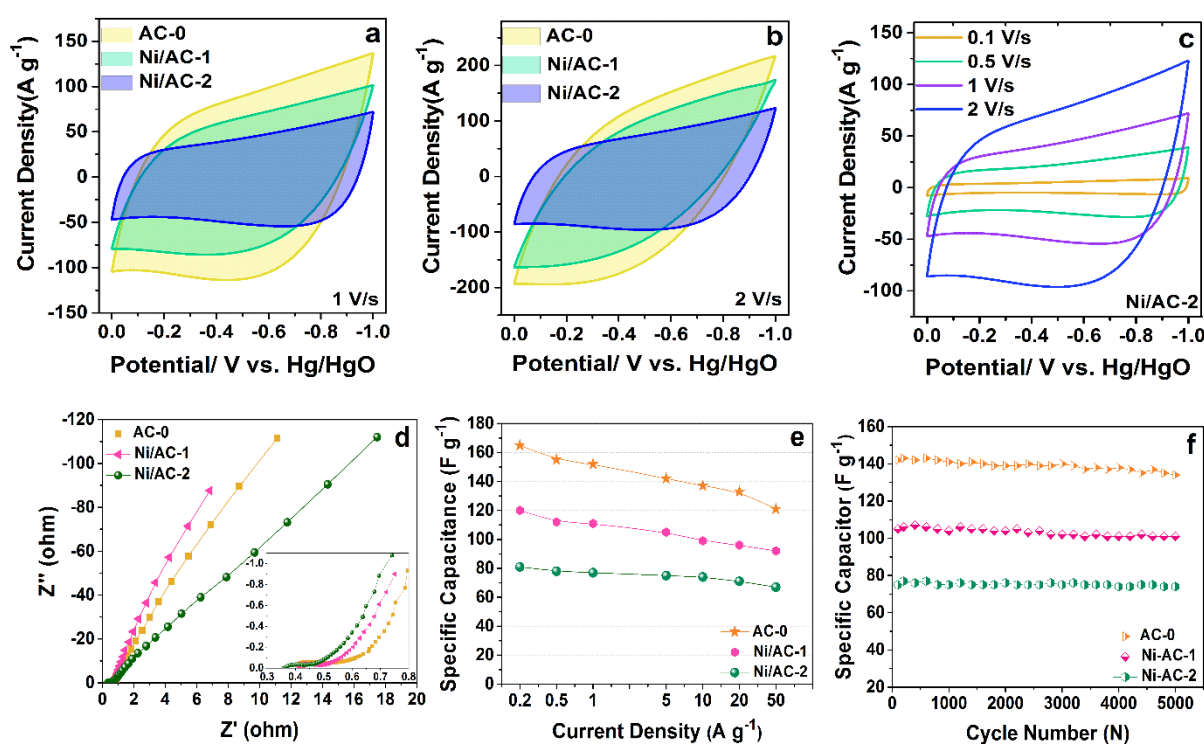


**Figure 5.** (a, b, c) CV curves, (d) AC impedance spectroscopy, (e) The specific capacitances at different current densities from 0.2 to 50  $\text{A g}^{-1}$  and (f) cycling performance at 5  $\text{A g}^{-1}$  of the sample electrodes.

Fig. 5d shows the Nyquist plots of all the electrodes from as-prepared materials. The EIS measurement was employed to quantitatively determine the equivalent series resistance (ESR) values for all the electrodes. The intercept at the  $Z'$ -axis is the combinational ohmic resistance ( $R_s$ ) at very high frequencies, resulting from the current collector, electrolyte, and active materials/current collector interface [24]. From the EIS data, the  $R_s$  of AC-0, Ni/AC-1 and Ni/AC-2 was determined to be 0.43  $\Omega$ , 0.41  $\Omega$  and 0.35  $\Omega$ , respectively. The Ni/AC-2 has a lower  $R_s$  value demonstrating a lower resistance with good electrical conductivity, which should be due to the special structure consistent with the

above CV results. Abundant interconnected channels in the nanostructures of the hybrid material have a large impact on the continuous electron transport pathways illustrated in Fig.1.

**Table 2.** Comparison of the performances of various nickel/carbon composite supercapacitors.

Materials	Capactiance (Fg <sup>-1</sup> )	Rate capability (%)	Circles deteriorati on (%)	References
Ni/AC-1	120 (0.2 A g <sup>-1</sup> )	76.7% (50 A g <sup>-1</sup> )	3.8 % (5000)	This work
Ni/AC-2	81 (0.2 A g <sup>-1</sup> )	82.7% (50 A g <sup>-1</sup> )	1.5 % (5000)	This work
Ni microtube /CNSs	89 (2.5 A g <sup>-1</sup> )	68.5 % (40 A g <sup>-1</sup> ) 1)	3 % (40000)	[11]
Ni/C	164 (0.25 A g <sup>-1</sup> )	~65 % (1.5 A g <sup>-1</sup> ) 1)	/	[12]
C800MOF	886 (2.5 A g <sup>-1</sup> )	84.4 % (40 A g <sup>-1</sup> ) 1)	13 % (1000)	[24]
Ni@C	152.7 (1 A g <sup>-1</sup> )	64.8% (10 A g <sup>-1</sup> )	9 % (2000)	[25]
G/Ni nanocomposite	275 (0.2 A g <sup>-1</sup> )	52.4 % (10 A g <sup>-1</sup> ) 1)	/	[31]
Ni@mesoporous carbon	912 (0.5 A g <sup>-1</sup> )	51.2 % (10 A g <sup>-1</sup> ) 1)	18 % (3500)	[32]
Ni-QDs /carbon	990 (0.5 A g <sup>-1</sup> )	47.3 % (10 A g <sup>-1</sup> ) 1)	15.1 % (5000)	[33]

Although, Ni/AC-2 exhibits a relatively low specific capacitance due to the metallic Ni content increase, this materials maintains the highest-stable capacity during high-rate operations as seen in the results from Fig. 5e, which shows the capacitance retention rates of the AC-0, Ni/AC-1 and Ni/AC-2

electrodes to be 73.3 %, 76.7 % and 82.7%, respectively, which is consistent with Table 1. As the working life is a highly significant factor of the electrodes used in electrochemical supercapacitors, the cyclic behavior of the electrode materials has been further studied to evaluate their stability by performing galvanostatic charge-discharge (GCD) at a current density of 5 A g<sup>-1</sup> for 5000 cycles (Fig. 5f). The capacitance deterioration of the AC-0, Ni/AC-1 and Ni/AC-2 electrodes was nearly 5.6 %, 3.8 % and 1.5 %, respectively. Compared to as synthesized MOFs-derived products, the performances of some other reported Ni/C nanocomposite electrode materials are detailed in Table 2. Although Ni/AC-1 and Ni/AC-2 have not demonstrated such high capacitances as the electrode materials with pseudocapacitance characteristics, however these two materials show excellent high-rate operations and cycling stabilities. These electrochemical results pertaining to the performance stability correspond to the above results, which could be attributable to the particular structure features of Ni/AC-2. The Ni nanoparticles in Ni/AC-2 have a low intrinsic resistance. In addition, the doping of with Ni could cause a polarization of the surrounding carbon surface to produce numerous graphitic shells, which may substantially improve the wettability of the porous carbon structure due to increasing the double-layer surface area accessible to the electrolyte.

#### 4. CONCLUSION

In summary, this material consists of uniform metallic Ni nanoparticles and partially graphitic porous carbon containing turbostratic graphitic shells. The performances of the electrochemical double-layer capacitor Ni/C nanocomposite derived from bimetallic MOFs were evaluated. The results showed excellent electrochemical performances especially during high-rate operations and long-term stabilities attributed to efficient ionic transportation and charge conductivity with low resistance. The present study may also be useful in the design of other composites with features desirable for electrochemical double-layer supercapacitor applications.

#### ACKNOWLEDGMENTS

This work was supported by a grant from the National Natural Science Foundation of China (No. 11280140) and the Project 2014DB03 from NPL, CAEP in China.

#### References

1. A. González, E. Goikolea, J.A. Barrena, R. Mysyk, *Renew. Sust. Energ. Rev.*, 58 (2016) 1189.
2. P. Sharma, T. Bhatti, *Energy Convers. Manage.*, 51 (2010) 2901.
3. M. Inagaki, H. Konno, O. Tanaike, *J. Power Sources*, 195 (2010) 7880.
4. X. Chen, R. Paul, L. Dai, *Natl. Sci. Rev.*, 4 (2017) 453.
5. B.G. Choi, M. Yang, W.H. Hong, J.W. Choi, Y.S. Huh, *ACS nano*, 6 (2012) 4020.
6. T. Chen, L. Dai, *Mater. Today*, 16 (2013) 272.
7. H. Ji, X. Zhao, Z. Qiao, J. Jung, Y. Zhu, Y. Lu, L.L. Zhang, A.H. MacDonald, R.S. Ruoff, *Nat. Commun.*, 5 (2014) 3317.
8. D.W. Wang, F. Li, M. Liu, G.Q. Lu, H.M. Cheng, *Angew. Chem. Int. Ed.*, 47 (2008) 373.
9. K. Jayawardena, Y. Tan, J. Fryar, H. Shiozawa, S. Silva, S. Henley, G. Fuge, B. Truscott, M. Ashfold, *Carbon*, 49 (2011) 3781.

10. L.G. Bettini, G. Divitini, C. Ducati, P. Milani, P. Piseri, *Nanotechnology*, 25 (2014) 435401.
11. X. Xia, Y. Zhang, Z. Fan, D. Chao, Q. Xiong, J. Tu, H. Zhang, H.J. Fan, *Adv. Energy Mater.*, 5 (2015) 1401709.
12. J. Li, E.-h. Liu, W. Li, X.-y. Meng, S.-t. Tan, *J. Alloys Compd.*, 478 (2009) 371.
13. Z. Xie, W. Xu, X. Cui, Y. Wang, *ChemSusChem*, 10 (2017) 1645.
14. M.H. Yap, K.L. Fow, G.Z. Chen, *Green Energy & Environment*, 2 (2017) 218.
15. X. Cao, C. Tan, M. Sindoro, H. Zhang, *Chem. Soc. Rev.*, 46 (2017) 2660.
16. Y.V. Kaneti, J. Tang, R.R. Salunkhe, X. Jiang, A. Yu, K.C.W. Wu, Y. Yamauchi, *Adv. Mater.*, 29 (2017) 1604898.
17. L. Wang, Y. Han, X. Feng, J. Zhou, P. Qi, B. Wang, *Coord. Chem. Rev.*, 307 (2016) 361.
18. G. Xu, P. Nie, H. Dou, B. Ding, L. Li, X. Zhang, *Mater. Today*, 20 (2017) 191.
19. J.-K. Sun, Q. Xu, *Energ. Environ. Sci.*, 7 (2014) 2071.
20. J.A. Botas, G. Calleja, M. Sánchez-Sánchez, M.G. Orcajo, *Langmuir*, 26 (2010) 5300.
21. H. Li, W. Shi, K. Zhao, H. Li, Y. Bing, P. Cheng, *Inorg. Chem.*, 51 (2012) 9200.
22. C.K. Brozek, M. Dincă, *J. Am. Chem. Soc.*, 135 (2013) 12886.
23. C.K. Brozek, M. Dincă, *Chem. Sci.*, 3 (2012) 2110.
24. M.-S. Wu, W.-H. Hsu, *J. Power Sources*, 274 (2015) 1055.
25. C. An, Y. Wang, L. Jiao, H. Yuan, *J. Mater. Chem. A*, 4 (2016) 9670.
26. X. Meng, C. Wan, Y. Wang, X. Ju, *J. Alloys Compd.*, 735 (2018) 1637.
27. B. Liu, H. Shioyama, T. Akita, Q. Xu, *J. Am. Chem. Soc.*, 130 (2008) 5390.
28. I. Afanasov, O. Shornikova, V. Avdeev, O. Lebedev, G. Van Tendeloo, A. Matveev, *Carbon*, 47 (2009) 513.
29. S. Han, F. Hou, X. Yuan, J. Liu, X. Yan, S. Chen, *Electrochim. Acta*, 225 (2017) 566.
30. M. Huang, X. Jiang, H. Zhang, H. Yin, X. Li, X. Ju, *J. Power Sources*, 272 (2014) 1.
31. N.A.M. Zaid, N.H. Idris, *Sci. Rep.*, 6 (2016) 32082.
32. H. Jiang, T. Sun, C. Li, J. Ma, *RSC Adv.*, 1 (2011) 954.
33. L. Su, J. Hei, X. Wu, L. Wang, Y. Wang, *ChemElectroChem*, 2 (2015) 1897.

© 2018 The Authors. Published by ESG ([www.electrochemsci.org](http://www.electrochemsci.org)). This article is an open access article distributed under the terms and conditions of the Creative Commons Attribution license (<http://creativecommons.org/licenses/by/4.0/>).